NANOSYSTEMS:
PHYSICS, CHEMISTRY, MATHEMATICS

Original article

Luginina A.A., et al. *Nanosystems: Phys. Chem. Math.*, 2025, **16** (6), 897–907.
http://nanojournal.ifmo.ru
DOI 10.17586/2220-8054-2025-16-6-897-907

Formation of NH_4MgF_3 and MgF_2 nanoparticles from magnesium hydroxycarbonate in ammonium hydrofluoride melt

Anna A. Luginina[1,a], Alexander A. Alexandrov[1,2,b], Darya S. Yasyrkina[1,c], Julia A. Ermakova[1,d], Victoria V. Tapero[1,3,e], Sergey V. Kuznetsov[1,f]

[1]Prokhorov General Physics Institute of the Russian Academy of Sciences, Moscow, Russia
[2]Kurnakov Institute of General and Inorganic Chemistry of the Russian Academy of Sciences, Moscow, Russia
[3]Department of Materials Science of Semiconductors and Dielectrics, National University of Science and Technology (MISIS), Moscow, Russia

[a]annaluginina@mail.ru, [b]alexandrov1996@yandex.ru, [c]darya.yasyrkina@gmail.com, [d]julia.r89@mail.ru,[e]kvv.padi@gmail.com, [f]kouznetzovsv@gmail.com

Corresponding author: A. A. Alexandrov, alexandrov1996@yandex.ru

ABSTRACT Ammonium fluorometalates with the perovskite structure NH_4MF_3 (M = 3d metals) are used for cathode materials and NH_4MgF_3 is used for solid electrolytes. There is only fragmentary information in the literature about the production of NH_4MgF_3 powder without available X-ray diffraction data. The conditions enable the synthesis of single-phase NH_4MgF_3 powder are proposed by reaction of magnesium hydroxycarbonate with ammonium hydrofluoride melt at a temperature of 220 °C. It has been established that the process is two-stage: the first reaction is the formation of the $(NH_4)_2MgF_4$ compound and the second reaction is the decomposition of $(NH_4)_2MgF_4$ at a temperature of 220 °C to NH_4MgF_3. Upon decomposition of NH_4MgF_3, anhydrous MgF_2 nanoparticles (28 ± 7 nm) are formed. The proposed method for obtaining single-phase NH_4MgF_3 opens up opportunities for studying its functional properties.

KEYWORDS ammonium fluorometalate, cubic perovskite structure, magnesium fluoride, nanoscale powders, NH_4MgF_3, ammonium hydrofluoride.

ACKNOWLEDGEMENTS The authors are grateful to I. A. Novikov for his help in conducting part the scanning electron microscopy. This research was performed using the equipment of the Shared Equipment Center of the Prokhorov General Physics Institute of the Russian Academy of Sciences and of the JRC PMR IGIC RAS. TEM studies were conducted using the equipment of the Centre for Collective Use "Materials Science and Metallurgy" (National University of Science and Technology "MISIS").

FOR CITATION Luginina A.A., Alexandrov A.A., Yasyrkina D.S., Ermakova J.A., Tapero V.V., Kuznetsov S.V. Formation of NH_4MgF_3 and MgF_2 nanoparticles from magnesium hydroxycarbonate in ammonium hydrofluoride melt. *Nanosystems: Phys. Chem. Math.*, 2025, **16** (6), 897–907.

1. Introduction

Ammonium fluorides (NH_4F and NH_4HF_2) react with many substances to form ammonium fluorometalates [1]. Structure and properties of cubic perovskite ammonium fluorometalates NH_4MF_3 (M = Mg and 3d transition element) have been intensively studied for several decades [2–8]. They crystallize in the cubic perovskite structure (sp. gr. $Pm\,\bar{3}m$, Z = 1) at room temperature, and under cooling, they undergo a structural phase transition into phases with lower symmetry such as tetragonal or orthorhombic crystal systems. NH_4MF_3 (M = Mn, Co, Ni) exhibit magnetic phase transitions at temperatures near or below the structural phase transitions [9–11]. These compounds are model objects for studying phase transitions in crystalline substances and determining the orientation of ammonium ions in the F- framework for various phases [12–19]. The perovskite structure allows for a fairly wide range of variation in the set of ions forming the lattice, thereby achieving the desired combination of material properties. In recent years, the NH_4MgF_3 and NH_4FeF_3 compounds have attracted attention as new solid electrolytes and cathode materials allowing for the direct introduction of lithium ions into the cubic perovskite structure [20, 21].

Unlike most of 3d transition elements, the complexing ability of magnesium is much lower and the formation of the compound NH_4MgF_3 can be explained by the proximity of the ionic radius of Mg^{2+} (0.72 Å) and the ionic radii of Mn^{2+} (0.83 Å), Fe^{2+} (0.78 Å), Co^{2+} (0.745 Å), Ni^{2+} (0.69 Å), and Zn^{2+} (0.74 Å) [22, 23]. NH_4MF_3 compounds were first synthesized by the reaction of MBr_2 with NH_4F in methanol [24, 25], and later obtained by pressing MF_2 with NH_4F upon heating [26]. Palacios et al. synthesized NH_4MF_3 by reacting a homogeneous mixture of solid MF_2 salts with NH_4HF_2 at 152 °C for several hours [4, 5]. Charpin et al. reported the synthesis of NH_4MgF_3 by heating a homogeneous mixture of magnesium carbonate powders with an unspecified excess of ammonium fluoride at 220 °C, followed by

washing off the excess NH_4F with formamide [27]. Ikrami et al. established the stepwise nature of the interaction of a mixture of ammonium fluoride or hydrofluoride powders with active magnesium oxide at a ratio of NH_4F:MgO = 4:1 and NH_4HF_2:MgO = 2:1 with the formation in both cases of intermediate compounds $(NH_4)_2MgF_4$ and NH_4MgF_3, stable in the temperature range of 160–180 °C and 220–230 °C, respectively [28]. However, they did not obtain the pure NH_4MgF_3 compound. The papers present various unit cell parameters of the compound NH_4MgF_3 prepared by "dry" methods (heating homogeneous mixtures of powders): a = 4.056 Å [5] and a = 4.06 Å [27]. Moreover, the diffraction pattern of the NH_4MgF_3 compound is not given in any papers. There is no information about the compound NH_4MgF_3 in the COD, JCPDS, CCDC, PDF-2 databases.

Ammonium hydrofluoride is more reactive than ammonium fluoride [1]. The reactions of interaction of ammonium fluoride or hydrofluoride with MgF_2 proceed according to the equations:

$$MgF_{2(s)} + NH_4HF_{2(s)} \rightarrow NH_4MgF_{3(s)} + HF_{(g)}, \quad (1)$$

$$MgF_{2(s)} + NH_4F_{(s)} \rightarrow NH_4MgF_{3(s)}. \quad (2)$$

The difference between the reactions is that reaction 1 occurs with the release of gaseous HF. An important difference is also that the interaction according to equation 1 occurs in the NH_4HF_2 melt, since its melting point is 126 °C [1]. As a result, the term "solid-phase reaction" which is often applied in the literature to processes involving NH_4HF_2, cannot be applied. In reality, heating processes inevitably occur in molten NH_4HF_2.

In addition to the described methods for synthesizing the NH_4MgF_3 compound, the literature contains no information whatsoever on the interaction of ammonium hydrofluoride with magnesium hydroxycarbonate, which exists in the form of a natural mineral, hydromagnesite, with the chemical formula $Mg_5(CO_3)_4(OH)_2\times4H_2O$.

The study of the conditions for the synthesis of the NH_4MgF_3 compound from magnesium hydroxycarbonate in melt of NH_4HF_2 with its subsequent conversion to magnesium fluoride is promising from the point of view of using the compound NH_4MgF_3 as a self-fluorinating precursor for the production of anhydrous magnesium fluoride.

Magnesium fluoride exhibits high transparency over an extremely wide spectral range, from vacuum ultraviolet to infrared [29–38]. Due to its high transparency and low refractive index, it has found wide application in various optical devices (e.g.: windows, lenses, filters, polarizers, and antireflective coatings for laser devices) [39–44].

The aim of the work is to study the synthesis of the NH_4MgF_3 compound by reacting magnesium hydroxycarbonate with a melt of ammonium hydrofluoride and subsequent thermal decomposition to prepare nanodispersed anhydrous MgF_2.

2. Experimental section

2.1. Materials and methods

The initial reagents such as magnesium hydroxycarbonate $Mg_5(CO_3)_4(OH)_2\times4H_2O$ (PrimeChemicalsGroup, Russia), ammonium fluoride NH_4F and ammonium hydrofluoride NH_4HF_2 (Fluoride Salts Plant, Perm, Russia) were analytical reagent grade. The number of water molecules in magnesium hydroxycarbonate was determined by thermogravimetric method using a MOM Q-1500 D derivatograph.

2.2. Synthesis

A homogeneous mixture of $Mg_5(CO_3)_4(OH)_2\times4H_2O$ and NH_4HF_2 powders was prepared by preliminary grinding of NH_4HF_2 powder in a fluoroplastic mortar with the gradual addition of $Mg_5(CO_3)_4(OH)_2\times4H_2O$ powder and grinding the mixture of powder for 15 min. The prepared homogeneous mixture of powders was transferred into a platinum crucible, covered with a lid and placed in an oven SNOL heated to 220 °C or 165 °C.

The conditions for sample synthesis are given in Table 1. Samples 2 and 3 were prepared in derivatograph upon thermogravimetric analysis (DTA-TG) at a heating rate of 10 °C/min. Sample 7–600 was obtained from Sample 7 by heating it at a rate of 10 °C/min to 600 °C without holding, followed by cooling.

2.3. Characterization

Diffraction patterns (XRD) were obtained on a Bruker D8 Advance powder X-ray diffractometer using CuKα radiation in the angular range from 10 to 140°C 2Θ, a signal acquisition time per point of 0.5–1 s, and sample rotation in the axial plane at a speed of 20 deg/min. Calculations of the unit cell parameters and coherent scattering regions (CSRs) were performed using TOPAS software.

Scanning electron microscopy (SEM) micrographs were obtained on a Tescan Amber scanning electron microscope using an Everhart-Thornley (E–T) detector and a low-energy back-scattered electron (LE-BSE) detector at accelerating voltages of 1–2 kV and a probe current of 300 pA. Particle sizes were determined using ImageJ software. Energy-Dispersive X-ray spectroscopy (EDX) was performed using an Oxford Instruments Ultramax EDS detector with an active area of 100 mm^2 at an accelerating voltage of 20 kV.

Thermogravimetric analysis was performed on a MOM Q-1500 D derivatograph in platinum crucibles in air. The heating and cooling rate was 10°C/min. Infrared spectroscopy was performed on an InfraLUM FT-08 spectrophotometer

TABLE 1. Sample synthesis conditions

Sample	Mg:F ratio	Temperature, °C	Synthesis duration, h
1	1:3	220	5
2 (DTA-TG)	1:3	600	0
3 (DTA-TG)	1:4	600	0
4	1:4	220	5
5	1:4	165	5
6	1:6	220	5
7	1:6	220	10
7–600	1:6	600	0
8	1:6	220	12

in the 4000–400 cm^{-1} range. Transmission electron microscopy (TEM) was performed on a JEM-2100 microscope (JEOL) with preliminary dispersion of the sample in water under ultrasound.

The magnesium content of the samples was determined by complexometric titration using disodium ethylenediamine-N, N, N′, N′-tetraacetic acid (di-Na-EDTA) in the presence of eriochrome black T indicator at pH = 10. The sample was first dissolved by boiling in a mixture of boric and hydrochloric acid solutions. The NH_4^+ content was determined by distillation using the Kjeldahl method, followed by titration with a hydrochloric acid solution in the presence of a mixed indicator (methyl red and methylene blue).

3. Results and discussion

The synthesis of NH_4MgF_3 compound was carried out at 220 °C, based on the results of thermogravimetric analysis, as well as on known literature data on the temperature range of stability of this compound of 220–230 °C [28] and the boiling point with simultaneous decomposition of NH_4HF_2 – 238 °C [45].

Magnesium hydroxycarbonate decomposes in several stages [46], Fig. 1a. The decomposition process begins at 206 °C, with a maximum endothermic effect at 273 °C and the removal of crystallization water with a loss of 18.6%. Then, the removal of chemically bound water occurs with a maximum at 410 °C and a loss of 7.2%. The exothermic effect at 487 °C corresponds to the formation of magnesium carbonate. Magnesium carbonate decomposes at 519 °C, losing 31.4% of its mass. The total mass loss of the sample is 57.2%.

In the DTA curves of the mixture of magnesium hydroxycarbonate powders with ammonium hydrofluoride at a ratio of Mg:F = 1:3 and 1:4, the first endothermic effect with a maximum of 124 °C is associated with the loss of adsorption water and the melting process of NH_4HF_2, Fig. 1b and Fig. 1c, respectively. The second endothermic effect, with a maximum at 213–219 °C, is caused by two processes: the onset of the removal of crystallization water from magnesium hydroxycarbonate and the reaction of interaction of initial reagents, initiated by the released water. The effect on the DTG, with a maximum at 265 °C, is apparently associated with the removal of crystallization water from magnesium hydroxycarbonate. Furthermore, the DTA curves for the mixture of magnesium hydroxycarbonate powders with ammonium hydrofluoride differ slightly for Mg:F ratios of 1:3 and 1:4.

The exothermic effect at 273 °C on the DTA curve with a ratio of Mg:F=1:3 is due to the crystallization of the intermediate compound, Fig. 1b. This intermediate compound in a mixture with MgF_2 was obtained by synthesis at 220 °C (Sample 1) Table 1. It is indexed in the hexagonal crystal system, space group $P6_3/mmc$, Table 2, Fig. 2c. The endothermic effect at 282 °C on the DTA curve is associated with the decomposition of the formed intermediate compound to magnesium fluoride. The exothermic effect at 297 °C is due to the crystallization of MgF_2. On the TG curve, the mass losses in the first (up to 126 °C), second (126 °C–226 °C), and third sections (226 °C–308 °C) are 7.3%, 45.3%, and 13.0%, respectively. The total mass loss was 65.6%, whilst the theoretical loss calculated for the production of MgF_2 is 65.4%.

After DTA-TG, a single-phase MgF_2 (Sample 2) was obtained, Fig. 2e, Table 2. Calculations of mass loss corresponding to the second and third sections on the TG curve, according to equations 3, 4, 5, are presented in Table 3. The phase composition of Sample 1 indicates the possible simultaneous occurrence of reactions at a ratio of Mg:F = 1:3 according to equations 4, 5:

$$Mg_5(CO_3)_4(OH)_2 \times 4H_2O + 7.5NH_4HF_2 \rightarrow 5NH_4MgF_3 + 4CO_2 + 2.5NH_3 + 10H_2O, \quad (3)$$

$$Mg_5(CO_3)_4(OH)_2 \times 4H_2O + 5NH_4HF_2 \rightarrow 5NH_4Mg(OH)F_2 + 4CO_2 + 5H_2O, \quad (4)$$

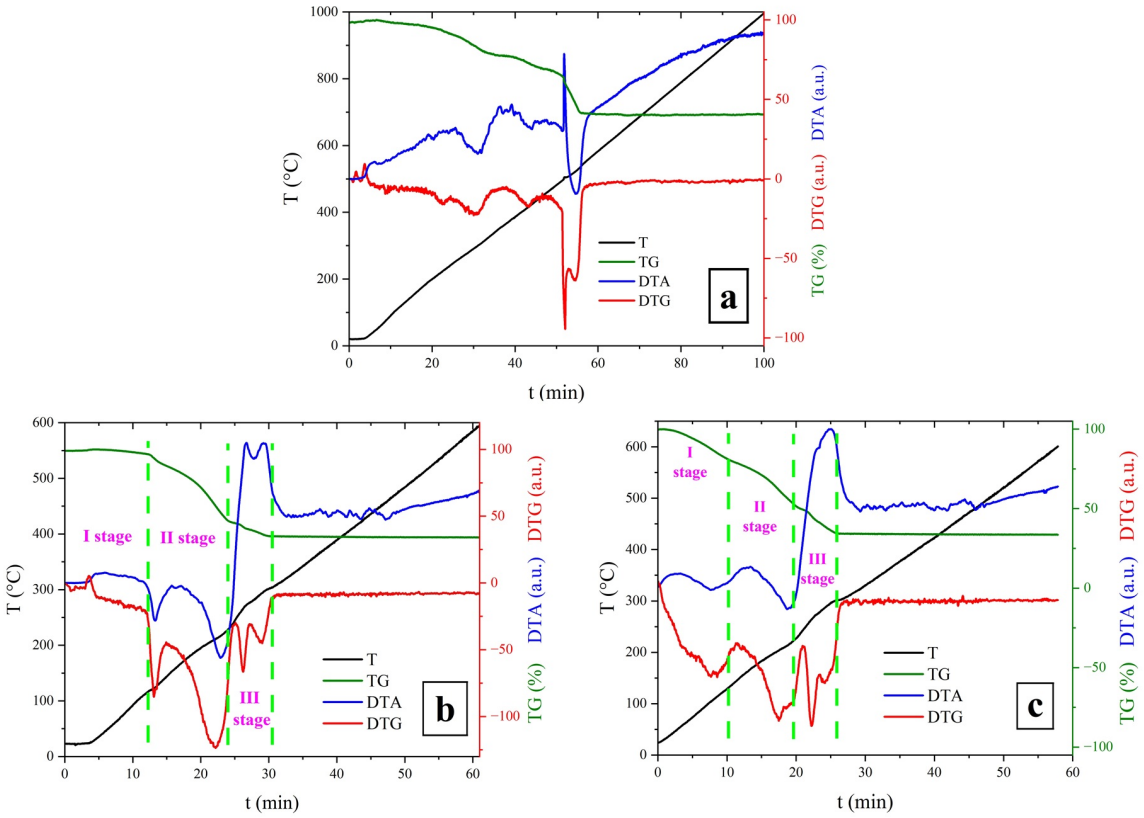

FIG. 1. Thermal analysis: a – magnesium hydroxycarbonate, b – mixtures of magnesium hydroxycarbonate powders with ammonium hydrofluoride at the ratio Mg:F=1:3 (Sample 2), c – same with Mg:F ratio 1:4 (Sample 3)

$$Mg_5(CO_3)_4(OH)_2 \times 4H_2O + 5NH_4HF_2 \rightarrow 5MgF_2 + 4CO_2 + 10H_2O. \quad (5)$$

The presence on the diffractogram of Sample 1, in addition to the reflections of the hexagonal phase (sp. gr. $P6_3/mmc$) and MgF_2, of the reflections of the compound $(NH_4)_2MgF_4$ (card PDF-2 card #00-050-0280) also indicates the possible occurrence of the reaction according to equation 6. Reflexes of the initial magnesium hydroxycarbonate are absent, Fig. 2b, Table 2.

$$Mg_5(CO_3)_4(OH)_2 \times 4H_2O + 10NH_4HF_2 \rightarrow 5(NH_4)_2MgF_4 + 4CO_2 + 10H_2O \quad (6)$$

On the DTG curve of a mixture of magnesium hydroxycarbonate and ammonium hydrofluoride powders with a Mg:F ratio of 1:4, a broad effect is observed at 203 °C with a shoulder at 220 °C, Fig. 1c. On the TG curve, the mass loss in the first (up to 126 °C) and second (126–226 °C) segments are 17.1% and 33.1%, respectively. The theoretical mass loss calculated using equation 6 (38.0%) does not correspond to that determined from the TG curve, which may indicate that reactions 4 and 6 proceed in parallel. The effect at 289 °C on the DTG curve is associated with the decomposition of the intermediate compounds formed into magnesium fluoride. The exothermic effect at 295 °C is due to the crystallization of MgF_2. The total mass loss was 66.3%, whilst the theoretical loss was 64.9%. After DTA-TG, a single-phase MgF_2 (Sample 3) was obtained, Fig. 2f, Table 2.

The XRD analysis confirmed the assumption that reactions (4) and (6) proceed in parallel. At a Mg:F ratio of 1:4, Sample 4 consists of cubic and hexagonal phases indicated on the diffractogram (Fig. 2d, Table 2) without reflections of the initial magnesium hydroxycarbonate. The presence of the cubic phase NH_4MgF_3 and the hexagonal phase confirm the assumption of simultaneous reactions according to equation (4) and (6). Further confirmation that the interaction proceeds according to equation (6) and not equation (3) is provided by the presence of an effect at 220 °C on the DTG curve of a mixture of magnesium hydroxycarbonate and ammonium hydrofluoride powders with a Mg:F ratio of 1:4, Fig. 1c. This effect indicates the decomposition of the $(NH_4)_2MgF_4$ compound formed according to equation 6 into a cubic phase NH_4MgF_3 [28]:

$$(NH_4)_2MgF_4 \rightarrow NH_4MgF_3 + HF + NH_3. \quad (7)$$

The chemical composition of the hexagonal phase of Samples 1 and 4 was not determined, since it was not isolated in pure form and this was not the objective of the study.

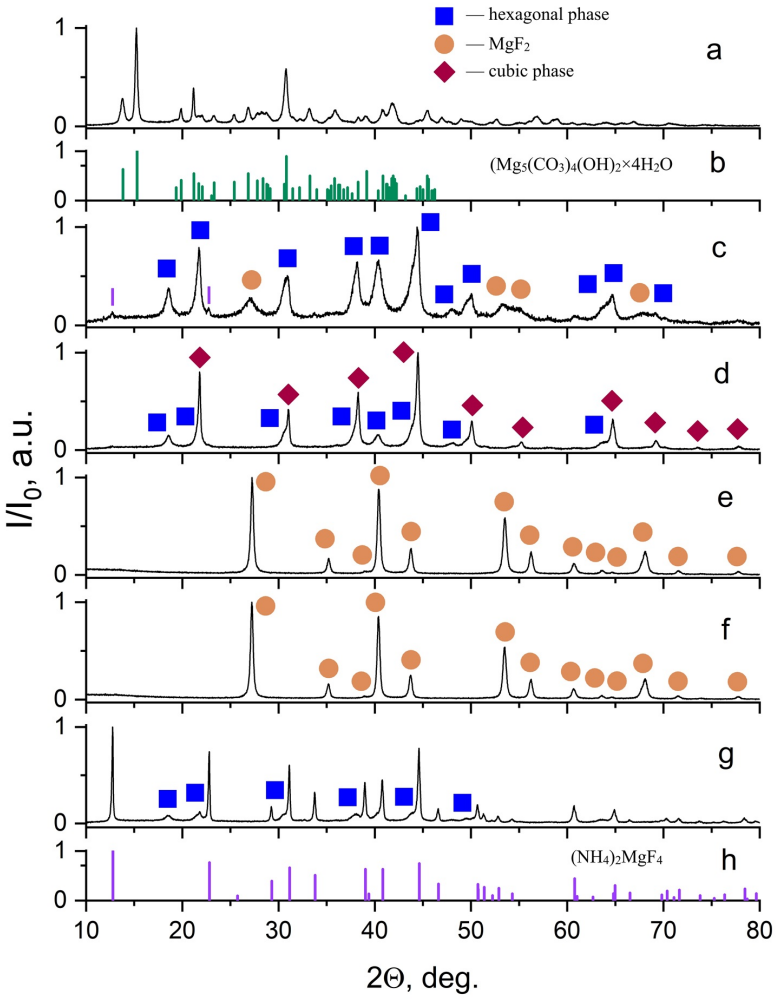

FIG. 2. XRD patterns: a – magnesium hydroxycarbonate, b – $Mg_5(CO_3)_4(OH)_5\times4H_2O$ card PDF-2 #00-025-0513, c – Sample 1, d – Sample 4, e – Sample 2, f – Sample 3, g – Sample 5, h – $(NH_4)_2MgF_4$ card PDF-2 #00-050-0280

The assumption made about the interaction of magnesium hydroxycarbonate with NH_4HF_2 according to equation 6 is further confirmed by the diffractogram of Sample 5, obtained at 165 °C with the ratio Mg:F = 1:4, Fig. 2g. The diffractogram of Sample 5 shows reflections of the $(NH_4)_2MgF_4$ compound and additional reflections indexated in the hexagonal symmetry (sp. gr. *P6₃/mmc*), Table 2. The diffractogram of sample with the ratio Mg:F = 1:5 contains reflections of the cubic phase and additional reflections of hexagonal phase (sp. gr. *P6₃/mmc*), see Supplementary Section (Table S1 and Fig. S1).

The XRD analysis traced the phase composition evolution of the products of the interaction between magnesium hydroxycarbonate and the NH_4HF_2 melt at 220 °C. In case of insufficient excess of ammonium hydrofluoride at the ratio:

1. Mg:F=1:3 results in formation of tetragonal MgF_2 (sp. gr. *P4₂/mnm*) and hexagonal phase (sp. gr. *P6₃/mmc*);

2. Mg:F=1:4 and 1:5 results in formation of cubic NH_4MgF_3 (sp. gr. *Pm* $\bar{3}$*m*) and hexagonal phase (sp. gr. *P6₃/mmc*).

A stepwise nature of the interaction between magnesium hydroxycarbonate and NH_4HF_2 melt has been established through the formation of the compound $(NH_4)_2MgF_4$ and its subsequent decomposition at a temperature of 220 °C to NH_4MgF_3. Thus, the excess amount of NH_4HF_2 required for the synthesis of NH_4MgF_3 compared to the stoichiometric amount according to equation (3) is associated not only with the compensation for the evaporation of NH_4HF_2 during heating, but also with the formation of the compound $(NH_4)_2MgF_4$.

Diffractogram of Sample 6 (Mg:F = 1:6) prepared by 5 h synthesis contains reflections of cubic NH_4MgF_3 and orthorhombic NH_4HF_2, Fig. 3a, Table 2. The increase in synthesis duration up to 10 and 12 h leads to evaporation of NH_4HF_2. There are only reflections of NH_4MgF_3 on Samples 7 and 8 diffractograms, Fig. 3(c,d), Table 2.

The NH_4^+ and Mg^{2+} content in chemical composition of NH_4MgF_3 compound (Sample 7) was determined by quantitative chemical analysis and EDX, Table 4 and 5.

TABLE 2. XRD analysis results of synthesized samples

Sample	Crystal system	Space group	Compound	Unit cell parameters, Å			Coherent scattered regions, nm
				a	b	c	
1	Tetragonal	*P*4$_2$/*mnm*	MgF_2	4.656(3)	–	3.04(1)	4(1)
	Hexagonal	*P*6$_3$/*mmc*	Composition not determined	5.824(3)	–	14.123(8)	15(1)
	Tetragonal*	*I*4/*mmm*	$(NH_4)_2MgF_4$	Traces			
2	Tetragonal	*P*4$_2$/*mnm*	MgF_2	4.624(1)	–	3.051(1)	18(1)
3	Tetragonal	*P*4$_2$/*mnm*	MgF_2	4.625(1)	–	3.051(1)	19(1)
4	Cubic	*Pm* $\bar{3}$*m*	NH_4MgF_3	4.072(1)	–	–	48(3)
	Hexagonal	*P*6$_3$/*mmc*	Composition not determined	5.846(1)	–	14.175(4)	10(1)
	Tetragonal*	*I*4/*mmm*	$(NH_4)_2MgF_4$	Traces			
5	Tetragonal*	*I*4/*mmm*	$(NH_4)_2MgF_4$	4.064(1)	–	13.860(1)	>100
	Hexagonal	*P*6$_3$/*mmc*	Composition not determined	5.848(2)	–	14.086(7)	6(1)
6	Cubic	*Pm* $\bar{3}$*m*	NH_4MgF_3	4.069(1)	–	–	64(3)
	Orthorombic**	*Pbmn*	NH_4HF_2	8.175(1)	8.419(1)	3.685(1)	44(1)
7	Cubic	*Pm*$\bar{3}$*m*	NH_4MgF_3	4.0663(1)	–	–	>100
7–600	Tetragonal	*P*4$_2$/*mnm*	MgF_2	4.623(1)	–	3.052(1)	25(1)
8	Cubic	*Pm*$\bar{3}$*m*	NH_4MgF_3	4.067(1)	–	–	92(4)

*$(NH_4)_2MgF_4$ PDF-2 card #00-050-0280

**NH_4HF_2 PDF-2 card #00-012-0302

TABLE 3. Mass loss according to TG during reagent interaction (Mg:F ratio = 1:3) compared to theoretical losses

Curve segment, Fig. 1b	Temperature range, °C	Mass loss, %			
		Experimental	Theoretical		
			3	4	5
II stage	126–226	45.3	45.1	34.9	65.4
III stage	226–308	13.0	20.6	19.4	-

TABLE 4. Results of quantitative chemical analysis of Samples 7 and 7–600

Sample	Compound	NH_4^+ content, wt. %		Mg^{2+} content, wt. %	
		Experimental	Theoretical	Experimental	Theoretical
7	NH_4MgF_3	18.1±0.5	18.1	24.0±0.7	24.5
7–600	MgF_2	–	–	39.2±0.7	39.0

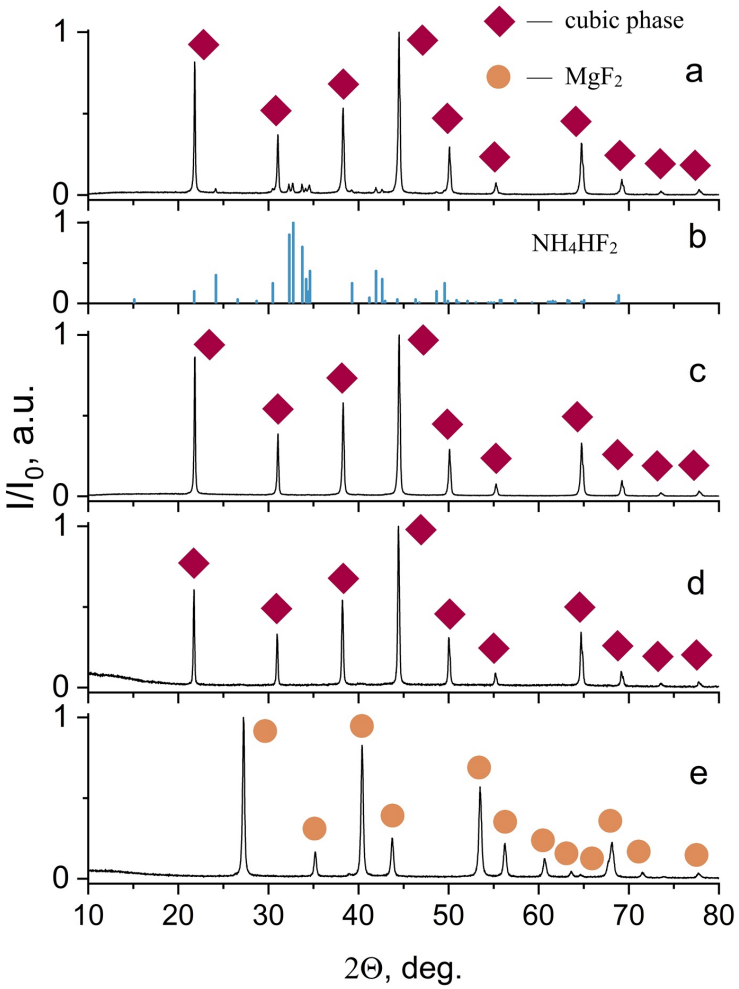

FIG. 3. XRD patterns: a – Sample 6, b – NH_4HF_2 PDF-2 card #00-012-0302, c – Sample 7, d – Sample 8, e – Sample 7–600

TABLE 5. Results of EDX analysis of Samples 7 and 7–600

Sample	Compound	N, at. %		F, at. %		Mg, at. %	
		Experimental	Theoretical	Experimental	Theoretical	Experimental	Theoretical
7	NH_4MgF_3	20±1	20.0	60±1	59.9	20±1	20.2
7–600	MgF_2	–	–	66±1	66.4	34±1	33.6

The formation of NH_4MgF_3 was also confirmed by FTIR-ATR (Fig. 4a). The IR spectrum of Sample 7 shows bands at 1461.2 cm^{-1} and 3220.9 cm^{-1}, corresponding to deformation vibrations (ν_3) and valence vibrations (ν_4) of the NH_4^+ ion [16, 47, 48].

The IR spectrum of Sample 7–600 does not include characteristic H_2O vibrations at ~1640 cm^{-1} and ~3400–3600 cm^{-1}. This observation confirms the absence of moisture traces in obtained MgF_2, Fig. 4b [49].

The DTA–TG data for synthesized sample 7 clearly confirm the XRD analysis results, indicating that the Sample 7 is a pure phase of NH_4MgF_3. The onset of the thermal decomposition according to DTA and TG is 280 °C with maximum at 294 °C and the end at 344 °C, Fig. 5a. Estimated experimental mass loss is 37.32%, which corresponds to theoretical losses 37.37% by following equation:

$$NH_4MgF_3 \rightarrow MgF_2 + HF + NH_3. \quad (8)$$

DTA-TG results in single-phase MgF_2 (Sample 7–600), Fig. 3e, Table 2. Composition of MgF_2 was confirmed by quantitative chemical and EDX analysis, Table 4 and 5.

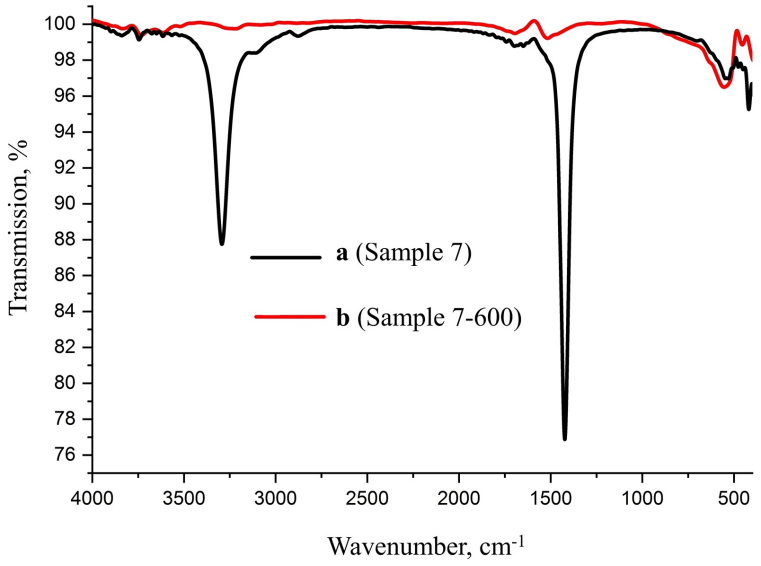

FIG. 4. FTIR-ATR spectra of: a – Sample 7, b – Sample 7–600

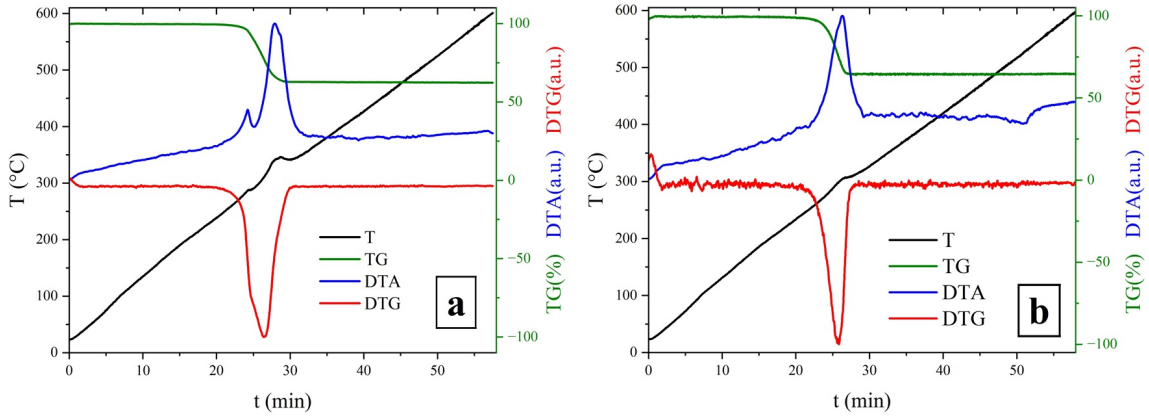

FIG. 5. DTA-TG results: a – Sample 7 and b – Sample 8

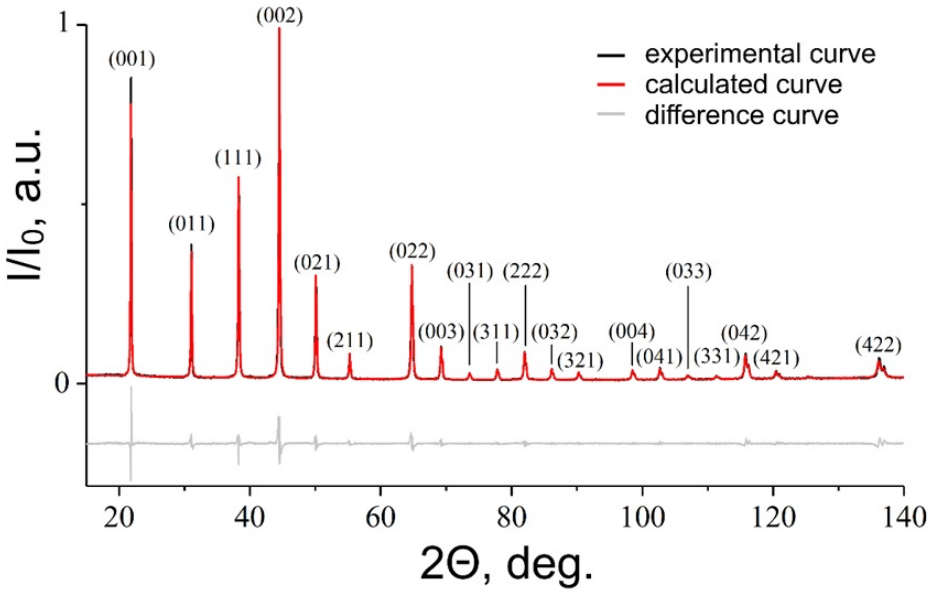

FIG. 6. Results of indexation of XRD pattern of Sample 7

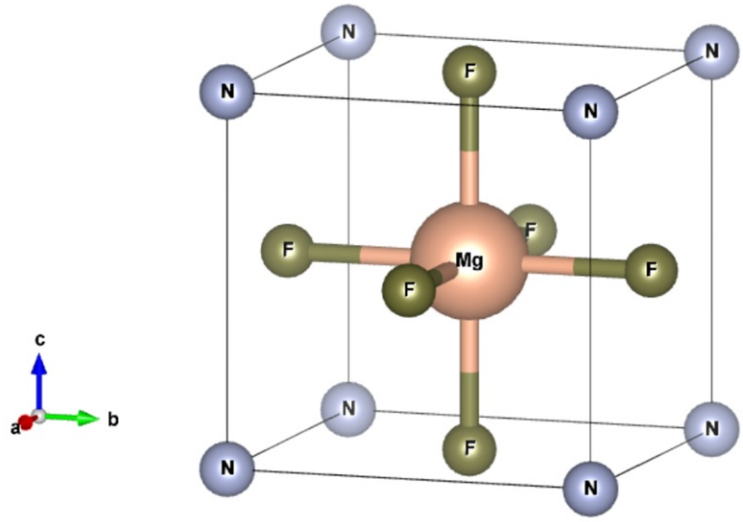

FIG. 7. Visualization of NH_4MgF_3 structure

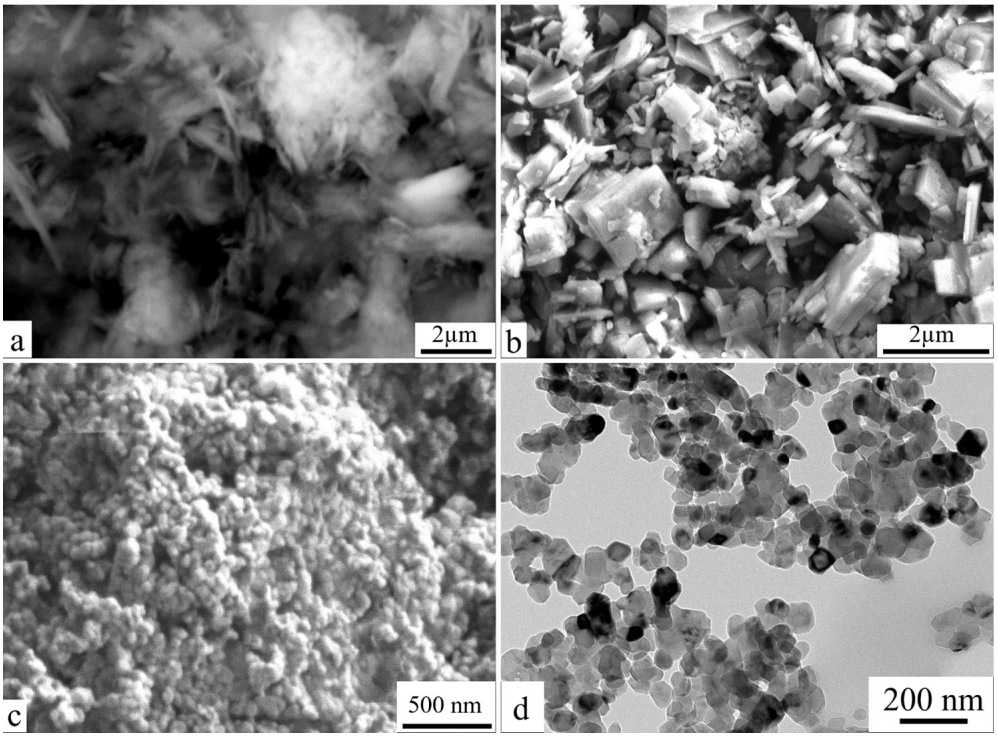

FIG. 8. The SEM/TEM microphotographs: a – magnesium hydroxycarbonate (SEM), b – Sample 7 (SEM), c – Sample 7–600 (SEM) and d – Sample 7–600 (TEM)

During the thermal decomposition of NH_4MgF_3 compound two processes occur simultaneously. Decomposition according to equation (8) the endothermic one and crystallization of the forming MgF_2 the exothermic one. Two exothermic peaks were observed on DTA curve of Sample 7 (Fig. 5a) and one exothermic peak were observed on DTA curve of Sample 8, Fig. 5b. Exothermic processes involving the crystallization of the magnesium fluoride phase are so intense that no endothermic processes were detected against their background.

The crystal structure of NH_4MgF_3 was refined on powder diffraction data in 15–140° 2Θ range using isostructural compound NH_4NiF_3 data [10]. Results of indexation of Sample 7 are presented in Fig. 6 and Supplementary section. The visualization of NH_4MgF_3 structure presented in Fig. 7.

The initial $Mg_5(CO_3)_4(OH)_2 \times 4H_2O$ consisted of flattened, long prismatic particles assembled into aggregates 400–1000 nm long and 30–50 nm thick, whose habitus was determined by the monoclinic structure of hydromagnesite, Fig. 8a. The initial habitus of hydromagnesite particles is not preserved during NH_4MgF_3 synthesis. The SEM image of Sample 7 shows nanoparticles with a 50–70 nm cube shape (Fig. 8b). The fusion of several primary nanoparticles of cubic

morphology with one crystallographic direction into larger particles (120–300 nm) that form micron-sized aggregates was recorded. The discrepancy between the sizes and the calculated values of the average crystal size (Table 2) may indicate the implementation of a non-classical mechanism of crystal formation through the oriented fusion of nanoparticles [50]. The heating of NH_4MgF_3 compound to 600 °C leads to significant changes. NH_4MgF_3 crystallites are destroying with the change of their chemical composition. The formation of rounded MgF_2 nanoparticle aggregates with a size of 71 ± 20 nm is observed, Fig. 8c. These aggregates are formed by nanoparticles with a size of 28 ± 7 nm that have a random orientation, Fig. 8d. The MgF_2 particle sizes determined from TEM micrographs agree reasonably well with the calculated values of the calculated scattering regions, Table. 2.

4. Conclusions

This study showed that NH_4HF_2 excess is required for the synthesis of the NH_4MgF_3. This is related not only to the compensation for NH_4HF_2 evaporation during heating, but also to the formation of a compound $(NH_4)_2MgF_4$. A stepwise nature of the reaction between magnesium hydroxycarbonate and molten ammonium fluoride through the formation of a compound $(NH_4)_2MgF_4$ which decomposes to NH_4MgF_3 at 220 °C has been established. The quantitative course of the reaction of magnesium hydroxycarbonate with molten ammonium hydrofluoride Mg:F=1:6 at 220 °C and 10 h with the formation of NH_4MgF_3 is shown. The fusion of several 50–70 nm primary nanoparticles with cubic morphology with formation of bigger particles with 120–300 nm size is observed.

At a Mg:F ratio lower than 1:6, the formation of multiphase products was observed, including $(NH_4)_2MgF_4$, NH_4MgF_3 and MgF_2 compounds and an impurity phase whose reflections are indicated in the hexagonal crystal system sp. gr. *P*6$_3$*/mmc*. During heat treatment NH_4MgF_3 is decomposing with formation of anhydrous nanocrystals MgF_2 with particle sizes 28 ± 7 nm.

References

[1] Rakov E.G., Mel'nichenko E.I. The properties and reactions of ammonium fluorides. *Russ. Chem. Rev.*, 1984, **53**, P. 851.

[2] Rüdorff W., Lincke G., Babel D. Untersuchungen an ternären Fluoriden. (II). Kobalt(II)- und Kupfer(II)-fluoride. *ZAAC*, 1963, **320**, P. 150–170.

[3] Patil K.S., Secco E.A. Complex fluorides with perovskite structure: thermal analyses, calorimetry, and infrared spectra. *Can. J. Chem.*, 1972, **50**, P. 1529–1530.

[4] Palacios E., Bartolomé J., Navarro R. et al. Heat capacity and N.M.R. study of the NH_4MgF_3 perovskite. *Ferroelectrics*, 1984, **55**, P. 287–290.

[5] Palacios E., Navarro R. Thermal properties of XMF_3: cubic perovskites. I. Heat capacity of NH_4MgF_3 and NH_4CdF_3. *J. Chem. Thermodynamics*, 1986, **18**, P. 1089–1101.

[6] Navarro R., Burriel R., Bartolomé J. et al. Thermal properties of XMF_3 cubic perovskites II. Heat capacity of NH_4ZnF_3 and $KZnF_3$. *J. Chem. Thermodynamics*, 1986, **18**, P. 1135–1146.

[7] Palacios E., Bartolomé J., Burriel R. et al. Proton-lattice relaxation in NH_4MF_3. *J. Phys.: Condens. Matter*, 1989, **1**, P. 1119–1132.

[8] Helmholdt R.B., Wiegers G.A., Bartolome J. Investigation of the structural phase transitions in the ammonium trifluorides of zinc, manganese and cobalt by means of X-ray and neutron diffraction. *J. Phys.: Condens. Matter*, 1980, **13**(27), P. 5081–5088.

[9] Bartolomé J., Navarro R., González D. et al. Magnetic properties of NH_4CoF_3. *Physica B+C*, 1977, **92**, P. 45–51.

[10] Plitzko C., Strecker M., Meyer G. Crystal structure of two modifications of ammonium trifluoro nickelate(II), NH_4NiF_3. *Z. Kristallogr. New Cryst. Struct.*, 1997, **212**, P. 3–4.

[11] Siebeneichler S., Dorn K.V., Smetana V. et al. A soft chemistry approach to the synthesis of single crystalline and highly pure $(NH_4)CoF_3$ for optical and magnetic investigations. *J. Chem. Phys.*, 2020, **153**, P. 104501-8.

[12] Bartolomé J., Navarro R., González D. et al. Librational and reorientational specific heats of NH_4^+ in NH_4ZnF_3 and NH_4CoF_3. *Physica B+C*, 1977, **92**, P. 23–44.

[13] Bartolomé J., Navarro R., González D., et al. Hindered rotational specific heat of NH_4^+ in the cubic perovskite NH_4ZnF_3. *Chem. Phys. Lett.*, 1977, **48**, P. 536–539.

[14] Steenbergen C., de Graaf L.A., Bevaart L. et al. Rotational motions of NH_4^+ groups in NH_4ZnF_3 studied by quasielastic neutron scattering. *J. Chem. Phys.*, 1979, **70**, P. 1450–1455.

[15] Rubin J., Bartolome J., Anne M. et al. The dynamics of NH_4^+ in the NH_4MF_3 perovskites: I. A quasielastic neutron scattering study. *J. Phys.: Condens. Matter*, 1994, **6**, P. 8449–8468.

[16] Plaza I., Rubin J., Laguna M.A. et al. Optical spectroscopy of the NH_4^+ - internal vibrations in the orthorhombic phase of NH_4MF_3 (M is Mn, Zn) perovskites. *Spectrochim. Acta, Part A*, 1996, **52**, P. 57–67.

[17] Smith D. The derivation of the rotational potential function from atom-atom potentials. II. Ammonium-fluorine compound. *J. Chem. Phys.*, 1987, **86**, P. 4055–4065.

[18] Laguna M.A., Sanjuan M.L., Orera V.M. et al. X-ray and Raman study of the low temperature NH_4MnF_3 structure; evidence of librational motion of the NH_4^+ ion. *J. Phys.: Condens. Matter*, 1993, **5**, P. 283–300.

[19] Aleksandrov K.S., Bartolome J., Gorev M.V. et al. Hydrostatic pressure effect on phase transitions in perovskites with ammonium cations. *Phys. Status Solidi B*, 2000, **217**, P. 785–791.

[20] Motohashi K., Matsukawa Y., Nakamura T. et al. Fast fluoride ion conduction of $NH_4(Mg_{1-x}Li_x)F_{3-x}$ and $(NH_4)_2(Mg_{1-x}Li_x)F_{4-x}$ assisted by molecular cations. *Sci Rep.*, 2022, **12**, P. 5955.

[21] Martin A., Santiago E.S., Kemnitz E. et al. Reversible insertion in $AFeF_3$ (A = K^+, NH_4^+) cubic iron fluoride perovskites. *ACS Appl. Mater. Interfaces*, 2019, **11**, P. 33132–33139.

[22] Shannon R.D. Revised effective ionic radii and systematic studies of interatomic distances in halides and chalcogenides. *Acta Cryst.*, 1976, **A32**, P. 751–767.

[23] Cotton F.A., Wilkinson G., Murillo C.A. et al. *Advanced Inorganic Chemistry*. Part 2. 6th ed. John Wiley and Sons, New York, 1999, 1355 p.

[24] Haendler H.M., Johnson F.A., Crocket D.S. The Synthesis of ammonium fluorometallates in methanol. *J. Am. Chem. Soc.*, 1958, **80**, P. 2662.

[25] Crocket D.S., Haendler H.M. Synthesis of fluorometallates in methanol. Some structure relationships. *J. Am. Chem. Soc.*, 1960, **82**, P. 4158–4162.

[26] Crocket D.S., Grossman R.A. The interaction between ammonium fluoride and metal fluorides as compressed powders. *Inorg. Chem.*, 1964, **3**, P. 644–646.
[27] Charpin P., Roux N., Ehretsmann J. Fluorures doubles de magnésium et d'ammonium. *C. R. Acad. Sci. Paris*, 1968, **267**, P. 484–486.
[28] Ikrami D.D., Ol'khovaya L.A., Luginina A.A. et al. Interaction of magnesium oxide with fluoride and ammonium hydrofluoride. *Russ. J. Inorg. Chem.*, 1977, **22**(3), P. 660–663.
[29] Guggenheim H. Growth of highly perfect fluoride single crystals for optical asers. *J. Appl. Phys.*, 1963, **34**, P. 2482–2485.
[30] Cotter T.P., Thomas M.E., Tropf W.J. *Magnesium Fluoride* (MgF_2). Handbook of Optical Constants of Solids, 1997, **2**, P. 899–918.
[31] Dodge M.J. Refractive properties of magnesium fluoride. *Appl. Opt.*, 1984, **23**, P. 1980–1985.
[32] Kitamura Y., Miyazaki N., Mabuchi T. et al. Birefringence simulation of annealed ingot of magnesium fluoride single crystal. *J. Cryst. Growth*, 2009, **311**, P. 3954–3962.
[33] Scott W. Purification, growth of single crystals, and selected properties of MgF_2. *J. Am. Ceram. Soc.*, 1962, **45**, P. 586–587.
[34] Hanson W.F., Arakawa E.T., Williams M.W. Optical properties of MgO and MgF_2 in the extreme ultraviolet region. *J. Appl. Phys.*, 1972, **43**, P. 1661–1665.
[35] Olsen A.L., McBride W.R. Transmittance of single-crystal magnesium fluoride and IRTRAN-1 in the 0.2 to 15-μ range. *J. Opt. Soc. Am.*, 1963, **53**, P. 1003–1005.
[36] Parsons W.E. Kodak Irtran infrared optical materials. *Appl. Opt.*, 1972, **11**, P. 43–48.
[37] Buckner D.A., Hafner H.C., Kreidl N.J. Hot-pressing magnesium fluoride. *J. Am. Ceram. Soc.*, 1962, **45**, P. 435–438.
[38] Chang C.S., Hon M.H., Yang S.J. The optical properties of hot-pressed magnesium fluoride and single-crystal magnesium fluoride in the 0.1 to 9.0 μm range. *J. Mater. Sci.*, 1991, **26**, P. 1627–1630.
[39] Volynec F.K. Optical properties and applications of optical ceramics. *Soviet Journal of Optical Technology*, 1973, **10**, P. 47–58.
[40] Zaidel A.N., Schrader E.D. *Vacuum Spectroscopy and Its Application*. Nauka, Moscow, 1980, 431 p.
[41] Voronkova E.M., Grechushnikov V.M., Distler G.I. et al. *Optical Materials for IR Technology*. Nauka, Moscow, 1965, 335 p.
[42] Zverev V.A., Krivopustova E.V., Tochilina T.V. *Optical materials*. Part 2. Textbook for Designers of Optical Systems and Devices. ITMO, Saint Petersburg, 2013, 248 p.
[43] Kuznetsov S.V., Alexandrov A.A., Fedorov P.P. Optical Fluoride Nanoceramics. *Inorganic Materials*, 2021, **57**(6), P. 555–578.
[44] Sun P., Jiang C., Jiang Y. et al. Structural, infrared optical and mechanical properties of the magnesium fluoride films. *Infrared Phys. Technol.*, 2024, **137**, P. 105184.
[45] Melnichenko E.I. *Fluoride Processing of Rare Earth Ores of the Far East*. DalNauka, Vladivostok, 2002, 268 p.
[46] Kashcheev I.D., Zemlyanoi K.G., Ustyantsev V.M., Voskretsova E.A. Investigation of thermal decomposition of natural and synthetic magnesium compounds. *Novye Ogneupory* (New Refractories), 2015, **10**, P. 28–35. (In Russ.)
[47] Oxton I.A., Knop O. Infrared Spectra of the Ammonium Ion in Crystals. I. Ammonium Hexachloroplatinate(IV) and Hexachlorotellurate(IV). *Can. J. Chem.*, 1975, **53**, P. 2675–2682.
[48] Knop O., Westerhaus W.J. Infrared spectra of the ammonium ion in crystals. Part XIV. Hydrogen bonding and orientation of the ammonium ion in fluorides, with observations on the transition temperatures in cubic cryolite, elpasolite, and perovskite halides. *Can. J. Chem.*, 1985, **63**, P. 3328–3353.
[49] Nakamoto K. *Infrared and Raman Spectra of Inorganic and Coordination Compounds*. John Wiley & Sons, Hoboken, New Jersey, 2009, 419 p.
[50] Ivanov V.K., Fedorov P.P., Baranchikov A.E., et al. Oriented attachment of particles: 100 years of investigations of non-classical crystal growth. *Russ. Chem. Rev.*, 2014, **83**(12), P. 1204–1222.

Submitted 14 November 2025; revised 19 November 2025; accepted 4 December 2025

Information about the authors:

Anna A. Luginina – Prokhorov General Physics Institute of the Russian Academy of Sciences, Vavilova str. 38, Moscow, Russia; ORCID 0000-0002-6564-5729; annaluginina@mail.ru

Alexander A. Alexandrov – Prokhorov General Physics Institute of the Russian Academy of Sciences, Vavilova str. 38, Moscow, Russia; Kurnakov Institute of General and Inorganic Chemistry of the Russian Academy of Sciences Leninskiy Prospekt, 31, Moscow, Russia; ORCID 0000-0001-7874-7284; alexandrov1996@yandex.ru

Darya S. Yasyrkina – Prokhorov General Physics Institute of the Russian Academy of Sciences, Vavilova str. 38, Moscow, Russia; ORCID 0000-0003-3053-4719; darya.yasyrkina@gmail.com

Julia A. Ermakova – Prokhorov General Physics Institute of the Russian Academy of Sciences, Vavilova str. 38, Moscow, Russia; ORCID 0000-0002-9567-079X; julia.r89@mail.ru

Victoria V. Tapero – Prokhorov General Physics Institute of the Russian Academy of Sciences, Vavilova str. 38, Moscow, Russia; Department of Materials Science of Semiconductors and Dielectrics, National University of Science and Technology (MISIS), Leninskiy Prospekt, 4, Moscow, Russia; ORCID 0009-0002-8771-5465; kvv.padi@gmail.com

Sergey V. Kuznetsov – Prokhorov General Physics Institute of the Russian Academy of Sciences, Vavilova str. 38, Moscow, Russia; ORCID 0000-0002-7669-1106; kouznetzovsv@gmail.com

Conflict of interest: the authors declare no conflict of interest.